Developments and Upgrades of Storage Ring

Improvement of Top-up Operation

Development of the Bunch current monitor [1]

The bunch current measurement is necessary for equalizing the bunch current of the filling pattern. At present, users demand that the non-uniformity of the bunch current should be less than 10%. To achieve this requirement, we developed the bunch current measurement system. We measured the waveform composed of 2436 RF buckets from a button pickup electrode using a 20 Gs/s oscilloscope. The bunch current is calculated from the minimum peak of the waveform for each bucket. Because the sampling rate (50 ps/point) is not sufficient to obtain the minimum pulse signal (width of approximately 300 ps), we interpolate the measured points and obtain accuracy of less than 1% compared with the measured value of DCCT for the filling pattern of a single bunch. It required about 27 seconds to measure entire bunch current. It is sufficient for top-up injection with a 1-minute interval, but if we reduce the measurement time further, we can stabilize the total beam current more precisely. We therefore improved the performance of the bunch current measurement system. We found that we could reduce the calculation time by utilizing the CPU of a Microsoft Windows computer interfaced with the oscilloscope instead of sending a large volume of data to the workstation. By using this scheme, the measurement time is reduced from 27 seconds to 10 seconds. We also implement function to measure the synchronous phase angle for each bunch, which is vital for time-resolving experiments. Figure 1 shows an example of the measured bunch currents and phase angles.

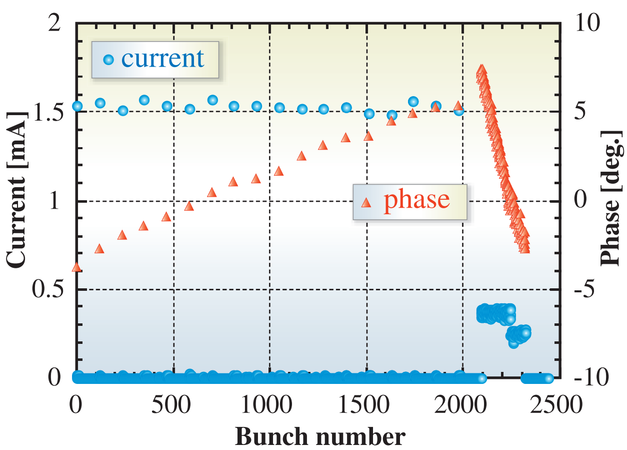

Fig. 1. An example of the measured bunch currents and phase angle in the case of filling mode of a 2/21-partially filled multi-bunch with 18-isolated bunches.

Suppression of Stored Beam Oscillation

Although the total stored current is made constant with high accuracy, the stored beam oscillation generated by the injection bump can cause fluctuations in the photon intensity at the experimental station. At present, the tilt of the bump magnet field is the main source of the vertical oscillation of the stored beam at the beam injection. The SPring-8 storage ring has four pulse bump magnets for beam injection. These magnets were made of 0.1-mm-thick laminated silicon steel of C-type configuration. If the fields of the bump magnets have a tilt against the direction perpendicular to the horizontal plane, the stored beam is kicked by the field and begins to oscillate in the vertical direction. The oscillation lasts until it decays out, thus, it may disturb the experiment that is sensitive to the photon intensity variation although the decay time is in tens of msec. To suppress the oscillation of the stored beam as much as possible, it is necessary to measure precisely the field directions of bump magnets. Using a search coil, we measured the horizontal magnetic field B_x. Then, the tilt angle of the magnetic field is measured by searching the angle at the minimum output voltage from the search coil. The tilt angle of the search coil was calibrated by a dipole magnet of H-type configuration, which has a precise mechanical relation between a pole face and a reference plane for alignment. Because the time evolution of the bump is very fast, we tried to measure the effect of the Eddy current. We measured the frequency dependence of the tilt angle of the magnetic field of the spare bump magnet, as shown in Fig. 2. We will continue to measure the tilt angle for all bump magnets. Based on the results, we will align the

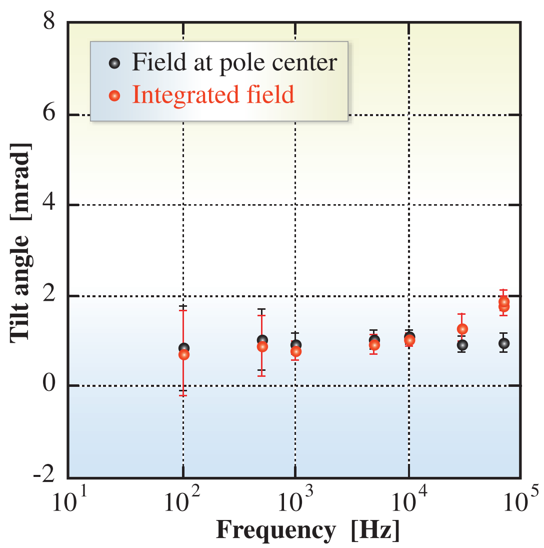

Fig. 2. Frequency dependence of the tilt angle for the bump magnet. Black points indicate the angle of the center of the magnet. Red points indicate the angle of the integrated field along the design orbit.

bump magnets. In addition, we will design the tilt control system for the bump magnets, which is used at a beam-based alignment to suppress the vertical oscillation.

Installation of Counter-Sextupole Magnets in Long Straight Sections

In the summer shutdown of 2000, we had locally removed and rearranged quadrupole and sextupole magnets to realize magnet-free long straight sections [2]. At that time, three unit cells were converted to the matching section, as shown in Fig. 3. The betatron phase advance in this section was set at $2\pi n$, where n is an integer (n=2 in the horizontal direction and n=1 in the vertical direction). Then, if no sextupole magnets are excited in the matching section, this part becomes "transparent," i.e., the electrons at the exit will have the same position and angle as they had at the entrance, and the periodicity of the ring can be kept high even after introducing long straight sections into the ring. This betatron phase matching is effective for obtaining large dynamic apertures and, hence, for realizing beam injection with high efficiency.

Such a phase condition, however, holds only for electrons with a design momentum. Because the beam is focused horizontally in the arc section by strong quadrupole magnets, the effect of chromatic aberration over the matching section is non-negligible. If the local chromaticity is uncorrected, off-momentum electrons receive a different focusing force from on-momentum ones, and betatron phase-slip occurs. As a result, the momentum acceptance of the ring becomes narrow and the Touschek beam lifetime becomes short. To correct the local chromaticity and enlarge the momentum acceptance, we have to excite sextupole magnets in the matching section. This, however, cause a harmful effect on the betatron phase matching and

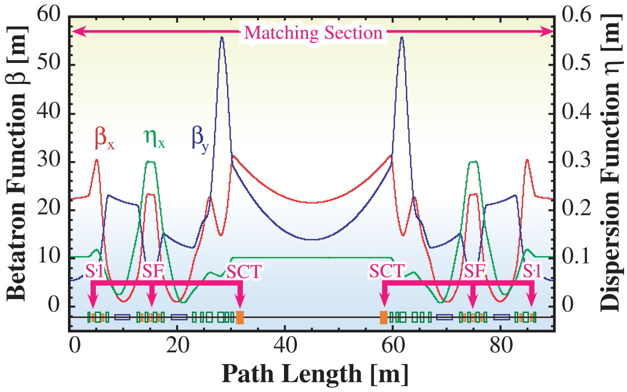

Fig. 3. Linear optics of the matching section and arrangement of the main magnets (blue: bending; green: quadrupole; orange: sextupole).

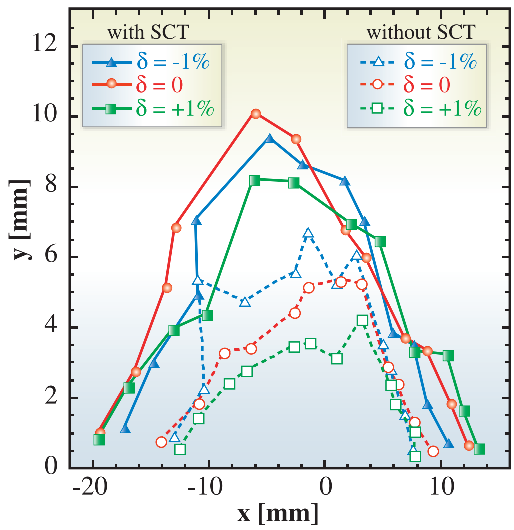

Fig. 4. Dynamic apertures at the injection point before (dashed lines) and after (solid lines) installing the counter-sextupole magnets. The momentum deviation is indicated by δ.

the dynamic aperture becomes smaller. At present, as a compromise, we excite only one family of sextupole in the matching section with a weak strength, labeled "SF" in Fig. 3, and both beam lifetime and injection efficiency are at acceptable levels for top-up operation.

To obtain longer beam lifetime and higher injection efficiency for stable top-up operation, we need to enlarge the dynamic aperture for on- and off-momentum electrons. For this purpose, we have recently developed a new scheme of local chromaticity correction. In this scheme, we use additional sextupoles which cancel nonlinear kicks due to SF in an approximate manner. These are "S1" and "SCT" in Fig. 3, and these are separated from SF by about π in the horizontal betatron phase. The magnet S1 has already been installed from the beginning, and SCT is a new one which we call counter-sextupole. The installation of counter-sextupole magnets will be completed in 2007.

After installing the counter-sextupole magnets, we can make the matching section "transparent" both for on- and off-momentum electrons. This also means that the optics will become more flexible; i.e., it will become easier to independently tune the local optics at each long straight section. This is another advantage of installing counter-sextupole magnets. In Fig. 4, we show the calculated dynamic apertures. The momentum deviation is indicated by δ. We see that the dynamic aperture is enlarged by introducing the counter-sextupole.

Renewal of BPM Electronics

The signal processing electronic circuits of the SPring-8 storage ring beam position monitors (BPM) were replaced during the summer shutdown of 2006. All of the 24 sets of circuits covering the entire ring were replaced at this time to improve the closed orbit distortion (COD) measurement performance.

The electronics are configured to measure the amplitude of the single component of 508.58 MHz, which is the RF acceleration frequency, in the signal induced on the electrodes by the electron beams (Fig. 5). The input signals from 12 electrodes of 3 BPMs are multiplexed in the switch-filter module, and processed in one common path of the circuits. One set of the circuits is composed of four of these paths. After the multiplexing stage, signals go through band-pass filters (BPF) to select the RF acceleration frequency component in the pickup signals. The selected narrow-band RF signals are amplified and down-converted to 250 kHz intermediate frequency (IF) signal, amplified with variable-gain IF amplifiers, and sampled by 16-bit 2MSPS (mega samples per second) ADCs. Finally, the signal amplitudes are calculated in digital signal processors (DSP) using the digital data sampled by ADCs. In addition, the DSP has the following three functions: calculating the beam positions, setting the gain of the IF amplifier and switching the multiplexer, and communicating with the control system of the accelerator complex.

During the usual operation for user experiments, the position data are averaged for 100 times in the DSPs to improve the position resolution. It takes about 3 seconds to process all of the BPM around the entire ring. Since the old circuits, which were used until the 2006 summer shutdown, require more than 20 seconds to measure beam positions of the entire ring, the measurement speed improved by a factor of 7.

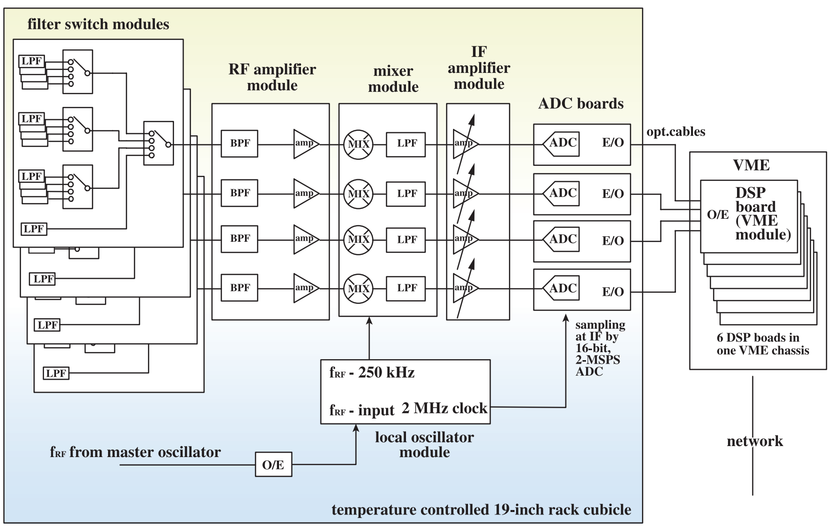

Fig. 5. Block diagram of one set of the signal processing circuits.

We continuously measured the COD every four seconds in order to estimate the position resolution; the differences in the two consecutive measurements were calculated to obtain the root mean square (r.m.s.) value of over a hundred measurements for each BPM. The r.m.s. value of each BPM includes the intrinsic resolution of the measurement system and also the movement of the COD between the two consecutive measurements. Figure 6 shows the r.m.s. values against the BPM serial numbers. A characteristic pattern appears in the graph. It seems that this pattern relates to the betatron function values. The square root of the betatron function values are also plotted in the same graph. The pattern observed in the r.m.s. values agrees well with the square root of the betatron function values when scaled and shifted properly.

We can postulate a model showing that the measured r.m.s. values can be decomposed to the intrinsic resolution and the effect of beam motion whose amplitude is proportional to the square root of the betatron function values at the BPM locations. According to the decomposition model, the measured r.m.s. values are expressed as

$$\sigma_i^2 = \sigma_0^2 + \sigma^2_{\mathrm{COD}_i} = \sigma_0^2 + \varepsilon_0 \times \beta_i\,,$$

where σ_i is the measured r.m.s. value of the i-th BPM, σ_0 is the intrinsic resolution, $\sigma_{\mathrm{COD}i}$ is the r.m.s. of the effect of the COD movement at the i-th BPM, β_i is the betatron function value at i-th BPM, and ε_0 is the proportionality constant. The assumptions in the model are that the intrinsic resolution is common to all of the BPM, the amplitudes of the COD motion are proportional to the square root of the betatron function values, and there is no correlation between the intrinsic resolution and the COD motion terms.

We plotted the squares of r.m.s. against the betatron function values as in Fig. 7, and carried out regression analysis with linear model as $\sigma^2 = a + b \cdot \beta$, where σ^2 is the measured r.m.s., β is the beta function value, a and b are the fitting parameters. The parameter a interests us; the

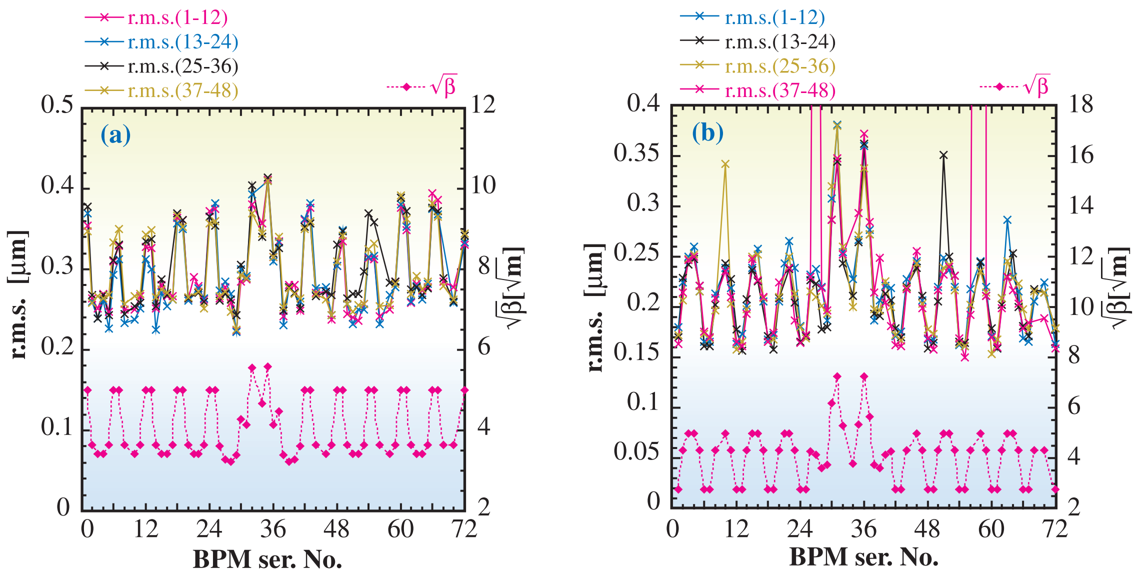

Fig. 6. The r.m.s. values of the difference in two consecutive COD measurements over 100 times against the serial number of BPMs (left axis). The plots are 4-folded, because the storage ring has a 4-fold symmetry in the lattice structure. The square root of the betatron function values are also plotted (left axis). **(a)** horizontal direction, **(b)** vertical direction.

obtained parameters are 0.017±0.002 μm^2 in the horizontal direction and 0.010±0.001 μm^2 in the vertical direction, respectively. From these values, we estimated the intrinsic resolution as 0.130±0.008 μm for horizontal and 0.100±0.005 μm for vertical directions. Rounding to one decimal place, the intrinsic resolution was found to be 0.1 μm.

For comparison, we performed a similar analysis for the data taken with the old signal processing circuits, and obtained a resolution 0.28±0.04 μm for the horizontal direction. For the vertical direction, we could not observe the distinct betatron function dependence pattern; the cause was not clear. Therefore, no values were obtained in the vertical direction by this method. By rounding to one decimal place, the resolution was found to be 0.3 μm for the old circuit. By comparing the intrinsic resolutions of the old and the new circuits, the resolution improved by a factor of three.

We observed bunch filling pattern dependence in the order of a few tens μm. The cause was attributed to the effect of the partial conduction of the diodes that were put to protect against very high voltage inputs to the multiplexer ICs; because of this, the linearity of the circuit response was degraded. The solution to this problem would be to put BPFs at the input to the multiplexer to eliminate the unnecessary components of the electrode signals, and lower the peak of the input voltage. The addition of the BPFs is expected to be carried out in a year or two. Further improvement is necessary to overcome the filling pattern dependence.

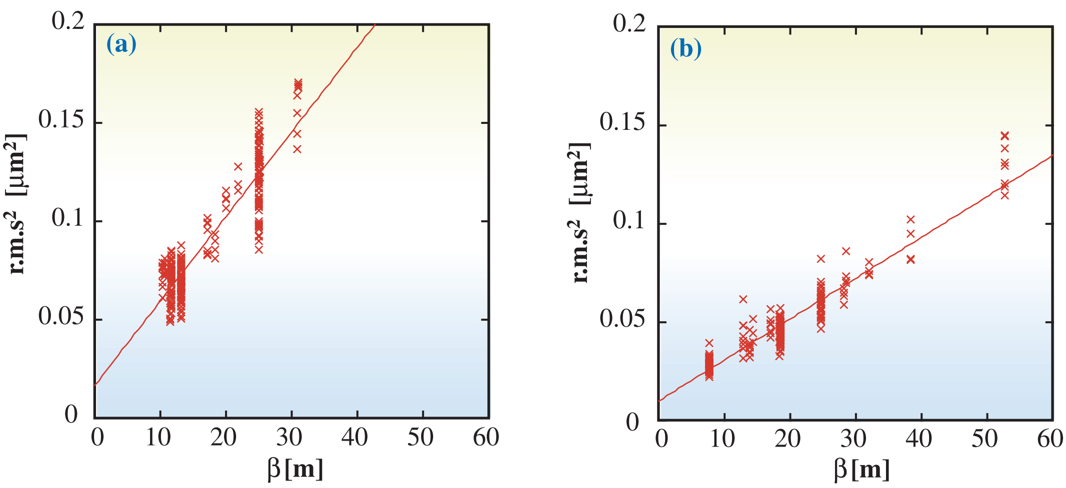

Fig. 7. The squares of measured r.m.s. values against betatron function values. The straight line is the fitting result with linear function. **(a)** horizontal direction, **(b)** vertical direction.

Development of Accelerator Diagnosis Beamlines

The accelerator diagnosis beamline I (BL38B2) has a bunch purity monitor to evaluate the purity of the main bunches of several-bunch operation modes [3] and an X-ray beam imager for beam emittance diagnosis [4]. The data acquisition system of the bunch purity monitor and the X-ray beam imager was developed for real-time beam monitoring. The bunch purity monitor is now continuously monitoring the electron beam of the user experiments under top-up injection. The continuous operation of the X-ray beam imager is suspended because of the degradation of the input photocathode of the X-ray zooming tube.

A study on the production of γ-ray photons in the energy range of 10 MeV has been performed at the diagnosis beamline I [5]. The MeV γ-rays are generated by the backward Compton scattering of optically pumped far-infrared (FIR) laser photons from 8 GeV electrons in the storage ring. Figure 8 shows the measured energy spectra under the conditions of "FIR laser on" and "FIR laser off". The MeV photons and synchrotron radiation less than 2 MeV were electrically discriminated by the detection circuits. Figure 8 also shows the net MeV γ-ray spectrum deduced by subtracting the "FIR laser off" spectrum from the "FIR laser on" spectrum. The estimated MeV photon production rate is $2{\times}10^3$ photons/sec per FIR laser output power of 1 W.

The construction of the accelerator diagnosis beamline II (BL05SS) is in progress. The front end and the radiation shielding hutches have already been completed, and now, the so-called edge radiation from the bending magnets upstream and downstream of the ID straight section of the beamline can be delivered to the optics hutch I. To study the coherent synchrotron radiation in the wavelength region comparable to the bunch length, the intensity of the microwave component of the edge radiation was measured as functions of the bunch length and the bunch current. A significant correlation between the microwave intensity and the bunch length was observed. To start the commissioning of the ID, which was installed in the summer of 2005, the steering magnets of the ID were tuned for various magnet gaps. The development of the vacuum components of the optics hutches I and II is in progress. The components of the optics hutch I, such as the movable mirror to pick off-the-edge radiation, the masks, the graphite filters, the metal filters, and the absorber, have been completed. The screen monitor and the double crystal monochromator, which is to be installed in the optics hutch II, are under development. The x- and y-slits to shape the input X-ray beam of the monochromator, which are to be added to the front end, are also under development.

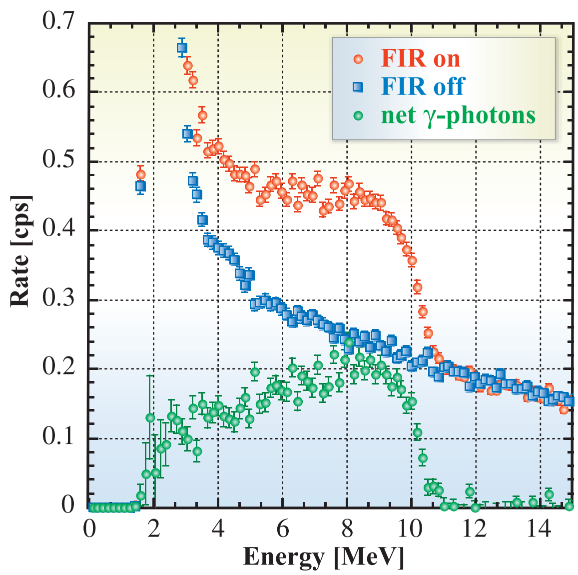

Fig. 8. Measured energy spectra of MeV γ-rays generated by backward Compton scattering.

To produce highly intense MeV γ-ray photons, an advanced plan of laser Compton scattering is in progress at the diagnosis beamline II, which has a straight section suitable for interaction between FIR laser photons and 8 GeV electrons. The expected production rate of MeV photons is more than 10^5 photons/sec. The construction of the laser clean room and the installation of the wave guide system for the transport of the FIR laser have been completed.

Development of New Gate Valve with a Comb-type RF Shield

One of the limitations of the bunch current is the increase in temperature of the finger-type RF shield of gate valves. The finger-type RF shield, which is made from BeCu, is attached for the smooth streaming of the wall current induced by the electron beam. The contact force of BeCu decrease because of the creep phenomena, if its temperature increases to 150°C. The reduction in contact force of BeCu induces more temperature increase, and finally, the finger-type RF shield will break, and the gate valve will not work. For example, the temperature of the finger-type RF shield increases to more than 80°C with the 203 bunches operation.

To realize the high-bunch current operation, it is necessary to develop a gate valve with a new type of RF shield. KEK already developed the gate valve with a comb-type RF shield, and it is used in the KEK B-Factory [6]. We tried to apply the comb-type RF shield to a new type of gate valve in collaboration of KEK (Fig. 9). A prototype of the gate valve with a comb-type RF shield will be manufactured by March 2007, and several tests will be scheduled.

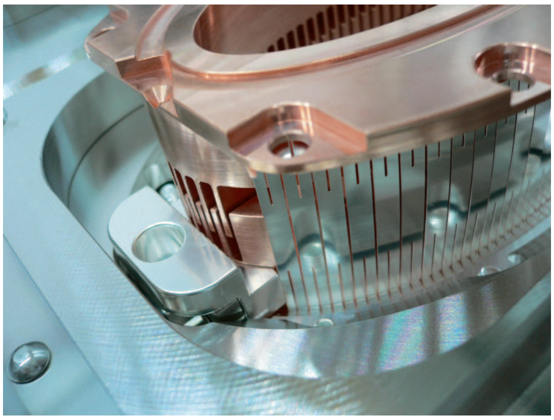

Fig. 9. Comb-type RF shield for SPring-8 gate valve.

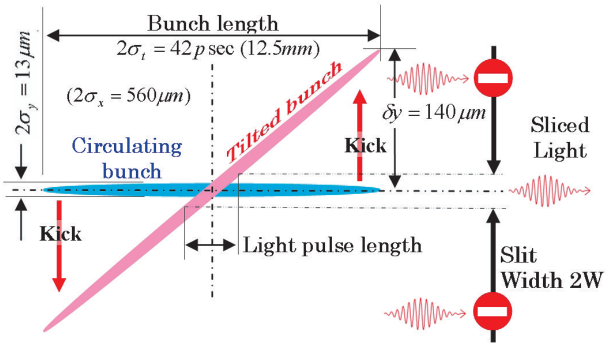

Fig. 10. Principle of FSX generation. A circulating electron bunch is kicked and tilted by RF deflectors. A portion of the emitted X-ray can pass through the slit. The bunch size and tilting are values for 8 GeV.

Development of Femtosecond Pulse X-ray Generation

The SPring-8 storage ring has a very small vertical bunch size. By using this feature, it is possible to generate a femtosecond pulse X-ray (FSX) by the bunch slicing method [7,8]. The achievable performance of the X-ray has been estimated for the operating conditions of the storage ring by installing four superconducting RF deflectors and a minipole undulator. The calculated pulse width, flux density and X-ray energy are 600 fsec in two standard deviations, 8.483×10^{15} photons/(sec • mrad^2 • 0.1%BW • 100 mA), and 10.7 keV, respectively, for 4 GeV operation.

On the other hand, problems are discussed and their countermeasures are developed to realize the FSX generation. The required phase stability among the RF deflectors was determined to be as small as 14.1 mdeg, and the mechanical vibration of cavities was considered as the main phase instability source. The phase stability of a superconducting cavity under operation at KEK was studied to confirm the analytical vibration model and to determine points of issue such as vibration sources. A high-speed and high-power phase shifter has been developed as a phase control device. Its phase control speed of 1 kHz at the 3 dB down point with a ±1-degree span has been obtained in a 300-kW power test. This year, the basic principle of FSX and a conceptual design are presented and details of the development will be reported next year.

The principle of FSX generation is shown in Fig. 10. The electrons in a bunch circulating in the storage ring have a three-dimensional Gaussian distribution. The bunch size in two standard deviations is 560 μm in the horizontal, 13 μm in the vertical, and 12.5 mm (42 psec) in the longitudinal or the traveling direction. If this bunch is tilted, as shown in Fig. 10, the X-ray emitted from each part of the bunch is vertically separated; the X-ray from the head of the bunch travels in the upper space, and that from the tail in the lower space. If we place a slit along the X-ray path, as Fig. 10, we can obtain a short pulse of X-ray emitted only at around the center of the bunch, and the other parts from the head and tail are blocked out. This method enables a storage ring to generate FSX whose pulse width is much shorter than its bunch length. In Fig. 10, the electrons do not collide with the slit if the slit is placed away from the electron orbit.

We have four 27-m magnet-free sections, called long straight sections, in the storage ring. Figure 11 shows an example of FSX generator installed in one of the long straight sections. In this figure, we configured four RF deflectors and an insertion device. The bunch enters into the FSX generator from "A" in Fig. 11; its head and tail are kicked to the opposite side by the first deflector "Def1." The bunch then rotates in the drift space "B", and its rotation is stopped by the second deflector "Def2." In the insertion device, the bunch emits X-ray in a stationary tilted position, and its tilting is returned back to the initial position inversely by "Def3" and "Def4," which are placed in a symmetric position as "Def2" and "Def1." The bunch has neither rotation nor tilting at exit "A' " of the FSX generator. Although a four-deflector design is shown here for easy understanding, another low-cost two-deflector design would be possible if "Def2" and "Def3" are replaced with two quadrupole magnets.

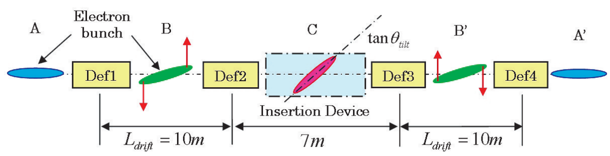

Fig. 11. Conceptual design of FSX generator. Four RF deflectors and an insertion device are installed in the 27-m-long straight section.